Performance of Disturbance Augmented Control Design in Turbulent Wind Conditions

Ahmet Arda Ozdemir*, Peter J. Seiler, Gary J. Balas

Department of Aerospace Engineering and Mechanics, University of Minnesota, Minneapolis, MN 55455, USA

Abstract

This paper investigates the use of disturbance models in the design of wind turbine individual pitch controllers. Previous work has used individual pitch control and disturbance models with the Multiblade Coordinate Transformation to design controllers that reduce the blade loads at the frequencies associated with the rotor speed. This paper takes a similar approach of using a disturbance model within the H_∞ design framework to account for periodic loading effects. The controller is compared with a baseline design that does not include the periodic disturbance model. In constant wind speeds, the disturbance model design is significantly better than the baseline design at canceling blade loads at the rotor frequencies. However, these load reduction improvements become negligible even under low turbulent wind conditions. The two controllers perform similarly in turbulent wind conditions because disturbance augmentation improves load reduction only at the multiples of the rotor frequency in the yaw and tilt moment channels whereas turbulence creates strong collective bending moments. In addition, turbulent wind contains energy across a broad frequency spectrum and improvements at multiples of the rotor frequency are less important in these conditions. Therefore inclusion of periodic disturbance models in the control design may not lead to the expected load reduction in fielded wind turbines.

Keywords: Individual Pitch Control, H infinity Control, Wind Turbines

*Corresponding author

Email addresses: arda@aem.umn.edu (Ahmet Arda Ozdemir), seiler@aem.umn.edu (Peter J. Seiler), balas@aem.umn.edu (Gary J. Balas)

1. Introduction

Demand for renewable energy is increasing rapidly with many governments setting aggressive goals towards greener energy alternatives. Wind energy plays an important role in this development as a promising renewable energy source and its success depends on the competitiveness of its cost per unit energy. The economics of wind power generation has driven the wind power industry to turbines of enormous size. Several issues arise due to the large dimensions including increased flexibility of the tower and blades and increased coupling between the turbine modes. Advanced control algorithms can be used to address vibration and loading issues, especially at above-rated wind speeds, and thus result in better fatigue reduction and lower maintenance costs.

A wind turbine operating in above-rated wind speeds (region 3) has the control objective of maintaining its rated power while minimizing structural loads on its blades, tower and the gearbox system. Turbulent wind conditions as well as persistent disturbances such as vertical wind shear, gravity and tower shadow are typical disturbances acting on the turbine. Conventionally, single-input single-output (SISO) classical control methods involving independent control loops are used for wind turbine control. A PID controller commanding collective blade pitch can be used to track desired constant rotor speed, while the generator torque is set accordingly to obtain rated power of the turbine. The generator torque command can be modified to add damping to the drive train torsion vibrations while collective pitch command can be modified to damp out tower fore-aft vibrations [1]. In addition to the SISO approaches, various multi-input multi-output (MIMO) control techniques such as Linear Quadratic Gaussian [2] and H_∞ [3] using individual pitch control (IPC) also have been investigated in the literature.

In addition to these methods, there are also MIMO controllers in the literature that are designed to eliminate the effects of persistent disturbances for load reduction. These controllers either use an observer to estimate the disturbances on the turbine in real time or include models of disturbances at the design stage of the controller. One common example of the estimator based approach is Disturbance Accommodating Control (DAC) [4, 5, 6]. DAC is an extension of LQR control that is based on estimating the persistent disturbances acting on the turbine. An example of the controllers that account for the effects persistent disturbances at design stage can be found in [7]. With this method, disturbance models are augmented to the plant

output to model the effects of the disturbances on system outputs. Instead of estimating the disturbances directly, the undesired effect of disturbances on system outputs are considered and controllers are designed to attenuate these effects.

All these linear control approaches require a linear representation of the nonlinear wind turbine system. The turbine is subjected to time-varying loads even in constant wind conditions because persistent disturbances such as tower shadow, gravity, shaft tilt e.g. and aerodynamic forces depend on the rotor position and structural flexibility. As a result, the wind turbine trim values are time-varying and periodic even in constant wind conditions. Real turbines always operate in varying wind conditions but assuming constant wind is a valuable approximation for understanding the turbine behavior around trim conditions. The amplitudes of these time-varying oscillations are significant for larger, more flexible turbines. The periodic behavior depends on the rotor position. Linearizations computed at each rotor position results in a periodic, linear time-varying (LTV) system with period equal to the rotor rotation period.

It is often desirable to transform the LTV control problem into an equivalent LTI problem to make use of well established linear time invariant (LTI) control techniques. There are various methods available in literature to obtain a LTI model from a LTV system. The simplest approach is to evaluate the periodic LTV system at a single constant rotor position. This approach ignores the periodic modal characteristics of the turbine and may not represent the nonlinear model well enough depending on the control problem. Averaging the state matrices over a single rotor period is another straightforward approach but there are no methods to determine the quality of model approximation [8]. Floquet theory [9] can be used to obtain a time-varying coordinate transformation that transforms a periodic LTV system into an LTI system while retaining all of the periodic modal characteristics. A drawback is that any physical intuition about the system states is lost during Floquet transformation. In this case, the eigenvectors of the resulting LTI system can be approximately related to the modes of the the physical system. Another modeling approach is to use the multi-blade coordinate (MBC) transformation [9, 10] to express the states, inputs and outputs of the turbine in a non-rotating coordinate frame. In general the MBC transformation does not directly result in an LTI system. However, the MBC approach usually yields a model that is weakly periodic and averaging of system matrices can result in a LTI model of sufficient accuracy [11]. The MBC transformation

is also known as the Coleman transformation or Fourier coordinate transformation in literature. Note that a reduced form of the MBC transform, called the $d-q$ transform, has also been applied to wind turbine control problems [2].

Recent turbine control techniques investigated in the literature commonly rely on the MBC transformation and disturbance model augmentation. Reference [12] investigates use of DAC and disturbance augmented H_∞ controllers for feed-forward and feedback controller design using LIDAR measurements. Reference [13] investigates use of Model Predictive Control and again relies on MBC and disturbance models. In this paper, the effects of disturbance model augmentation with the MBC are investigated for a standard Region 3 controller design. Potential benefits of disturbance augmentation has been investigated rather than posing a new controller architecture. The effects of the turbulence on the blade load reduction problem is also investigated and an attempt made to identify the performance bottlenecks. For this design, a periodic LTV system model of the nonlinear wind turbine dynamics is obtained by linearization of the wind turbine model as a function of the rotor angle. The periodic LTV system is approximated by an LTI system using the MBC transformation and averaging the resulting state matrices over one rotor rotation period. Oscillations in the trim operating points are modeled as disturbances of known frequencies and magnitudes acting on the output of the linear system. A H_∞ optimal controller designed on the disturbance augmented plant is compared with a baseline design that does not include the periodic disturbance model.

The paper has the following structure: Section 2 describes the nonlinear model used in this paper and explains the derivation of the LTI model. Section 3 explains the control problem formulation and design in detail. The linear analysis and nonlinear simulation results are presented in Section 4. Conclusions are presented in Section 5.

2. Wind Turbine Model

2.1. Nonlinear Wind Turbine Model

Nonlinear simulations presented in this work are performed using FAST [14], which stands for Fatigue, Aerodynamics, Structures and Turbulence modeling. FAST is a publicly available nonlinear aeroelastic turbine simulation code developed by National Renewable Energy Laboratory. FAST uses the assumed modes method for the flexible structural dynamics of the

system. Blade element momentum theory is used to calculate the aerodynamic loads using AeroDYN [15]. The wind turbine considered in this paper is the WindPACT 1.5MW horizontal axis, 3-bladed upwind turbine whose parameters are distributed with the FAST package.

FAST can model onshore wind turbines with a total of 22-24 degrees of freedom (DOF). This full order model includes first and second tower fore-aft and side-to-side bending modes, first and second flapwise bending modes of blades, first edgewise bending modes of blades, drivetrain torsion, generator position and nacelle yaw angle. Only a subset of these available DOF are chosen for the control design to reduce the complexity of the design. First, the yaw dynamics of the system are ignored since typically yaw motion and yaw actuators have time constants considerably larger than pitch actuators and generator torque control. Generator torque is not included as a control input and is held constant in this individual pitch control study. High frequency dynamics of the system that lie beyond the bandwidth of pitch actuators are also eliminated since the pitch actuators do not have enough control authority on these dynamics. These neglected dynamics include first edgewise and second flapwise bending modes of the blades, second tower fore-aft and side-to-side bending modes and drivetrain torsion. The final step is to eliminate the tower first side-to-side mode for the scope of this work. Even though IPC algorithms can affect this mode, side-to-side motion has limited effect on blade fatigue and it is eliminated for model reduction. During the control design no performance demands are imposed on the modes deleted from the system. The resulting simplified five degree-of-freedom system includes rotor position, first tower fore-aft bending mode and first flapwise bending mode for each blade. Note that the collective pitch action has a significant effect on tower fore-aft motion and in order to avoid destabilizing this lightly damped mode it is important to include it in control design [1]. This reduced order linear model is used for control design. Simulations are performed on high order nonlinear turbine model.

The five DOF nonlinear wind turbine modeled in FAST is represented by Equations (1) and (2). A block diagram of the wind turbine model is shown in Figure 1.

$$\ddot{q} = f(\dot{q}, q, u, F, t) \tag{1}$$

$$y = g(\dot{q}, q, u, F, t) \tag{2}$$

where $q \in R^5$ and $\dot{q} \in R^5$ are the turbine states, $u \in R^4$ is the control input, $F \in R^1$ is the wind disturbance and $y \in R^4$ is the measurement vector. The

variables are defined as:

$$q = \begin{bmatrix} q_1 \\ \psi_r \\ q_3 \\ q_4 \\ q_5 \end{bmatrix} = \begin{bmatrix} \text{Tower } 1^{st} \text{ Fore-Aft Bending Mode Tip Disp. (m)} \\ \text{Rotor position from Blade 1 Upwards Position (rad)} \\ \text{Blade 1 } 1^{st} \text{ Flapwise Bending Mode Tip Disp. (m)} \\ \text{Blade 2 } 1^{st} \text{ Flapwise Bending Mode Tip Disp. (m)} \\ \text{Blade 3 } 1^{st} \text{ Flapwise Bending Mode Tip Disp. (m)} \end{bmatrix} \tag{3}$$

$$u = \begin{bmatrix} \theta_1 \\ \theta_2 \\ \theta_3 \end{bmatrix} = \begin{bmatrix} \text{Blade 1 Pitch Angle (rad)} \\ \text{Blade 2 Pitch Angle (rad)} \\ \text{Blade 3 Pitch Angle (rad)} \end{bmatrix} \tag{4}$$

$$F = \begin{bmatrix} V_w \end{bmatrix} = \begin{bmatrix} \text{Horizontal Hub-Height Wind Speed (m/s)} \end{bmatrix} \tag{5}$$

$$y = \begin{bmatrix} \Omega \\ M_1 \\ M_2 \\ M_3 \end{bmatrix} = \begin{bmatrix} \text{Rotor Speed (rpm)} \\ \text{Blade 1 Bending Moment at Blade Root (kN m)} \\ \text{Blade 2 Bending Moment at Blade Root (kN m)} \\ \text{Blade 3 Bending Moment at Blade Root (kN m)} \end{bmatrix} \tag{6}$$

The generator torque input is held constant in this study hence it is not listed in the vector u in Eq. 4. The system outputs, vector y in Eq. 6, are selected to include a realistic sensor configuration for the study. Rotor speed measurement is commonly available on turbines and load sensors are becoming more popular due to their increasing reliability and low costs. In addition, implementation of controllers obtained through the MBC transformation requires knowledge of the rotor position even though it is not included in y measurement vector described. Rotor position measurement is also readily available in many turbines.

2.2. Linear Model

FAST has the capability of producing linear turbine models through numerical perturbation of system equations (1) and (2). The nonlinear system is first simulated under steady wind conditions until the turbine reaches a trim operating trajectory. The system is linearized around this trim trajectory. The trim operating condition is a periodic trajectory $\bar{q}(t)$ that satisfies Equation (7).

$$\begin{aligned} \ddot{\bar{q}} &= f(\dot{\bar{q}}, \bar{q}, \bar{u}, \bar{F}, t) \\ \bar{y} &= g(\dot{\bar{q}}, \bar{q}, \bar{u}, \bar{F}, t) \end{aligned} \tag{7}$$

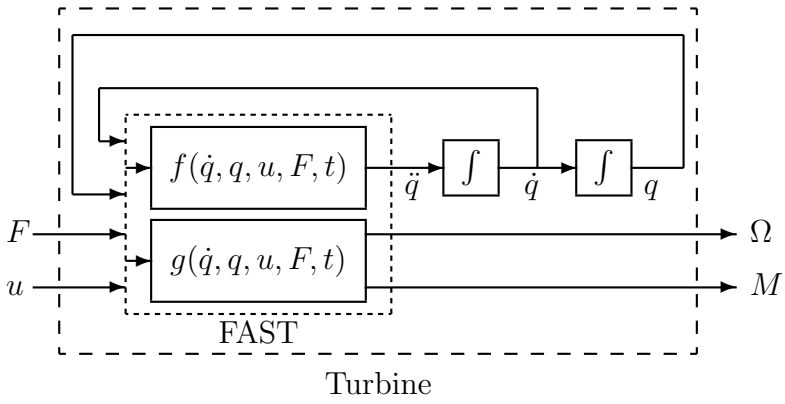

Figure 1: FAST Nonlinear System Block Diagram

$\bar{q}(t)$ is periodic in the rotor rotation period T, i.e. $\bar{q}(t+T) = \bar{q}(t)$. The wind input $\bar{F}$ and blade pitch angles $\bar{u}$ are held fixed at the trim values specified in Table 1. If the oscillations in $\bar{q}$ have small amplitude, the average state over one period can be assumed to be a constant trim condition without introducing large errors [16]. The effect of the periodic trajectory is not neglected in this paper. Rather, it is included as a periodic disturbance on the turbine. A linear time-varying model is obtained by linearizing the nonlinear system (Equations (1) and (2)) around $\bar{q}(t)$. The resulting equations have the form of Equation (8).

$$\begin{aligned} \dot{x} &= A(\bar{\psi}_r(t))x + B(\bar{\psi}_r(t))\Delta u + B_d(\bar{\psi}_r(t))\Delta F \\ \Delta y &= C(\bar{\psi}_r(t))x + D(\bar{\psi}_r(t))\Delta u + D_d(\bar{\psi}_r(t))\Delta F \end{aligned} \tag{8}$$

where

$$\begin{aligned} x = \begin{bmatrix} \Delta q \\ \Delta \dot{q} \end{bmatrix} &= \begin{bmatrix} q - \bar{q} \\ \dot{q} - \dot{\bar{q}} \end{bmatrix} \\ \Delta u &= u - \bar{u} \\ \Delta F &= F - \bar{F} \\ \Delta y = y - \bar{y} &= \begin{bmatrix} \Delta\Omega \\ \Delta M_1 \\ \Delta M_2 \\ \Delta M_3 \end{bmatrix} \end{aligned} \tag{9}$$

Since the trim trajectories are periodic, $\bar{\psi}_r(t) = \bar{\psi}_r(t+T)$, the system equations given by Equation (8) are also periodic. The operating conditions used for the linearization are listed in Table 1.

Table 1: Trim Conditions

Description	Value
Mean wind speed, $\bar{F}$	18.0 m/s
Vertical shear factor	0.2
Rotor speed, $\bar{\Omega}$	2.15 rad/s
Collective blade pitch, $\bar{u}$	0.3352 rad
Generator torque (High Speed Side)	8377.0 Nm

The linear and nonlinear wind turbine equations of motion presented are derived using a variety of coordinate frames. Reference [14] contains detailed figures of the coordinate frames used in turbine equations of motion. While quantities associated with the tower and rotor are expressed in an earth fixed coordinate frame, quantities that belong to individual blades are defined in a frame that rotates with the rotor. For instance, blade flapwise bending mode tip displacements are defined with respect to a rotating coordinate frame attached to the blade. The MBC transformation takes the system states, inputs and outputs defined in a mixed coordinate system (both rotating and non-rotating) and expresses them in a purely non-rotating coordinate frame.

The triplets of states, inputs, and outputs of the linear system that are expressed in a rotating frame are transformed as:

$$\begin{bmatrix} q_3^{nr} \\ q_4^{nr} \\ q_5^{nr} \end{bmatrix} = \mathbf{T}^{-1}(\bar{\psi}_r(t)) \begin{bmatrix} q_3 \\ q_4 \\ q_5 \end{bmatrix}, \begin{bmatrix} \theta_1^{nr} \\ \theta_2^{nr} \\ \theta_3^{nr} \end{bmatrix} = \mathbf{T}^{-1}(\bar{\psi}_r(t)) \begin{bmatrix} \theta_1 \\ \theta_2 \\ \theta_3 \end{bmatrix}, \begin{bmatrix} M_{avg}^{nr} \\ M_{tilt}^{nr} \\ M_{yaw}^{nr} \end{bmatrix} = \mathbf{T}^{-1}(\bar{\psi}_r(t)) \begin{bmatrix} M_1 \\ M_2 \\ M_3 \end{bmatrix} \tag{10}$$

where

$$\mathbf{T}^{-1}(\bar{\psi}_r(t)) = \frac{1}{3} \begin{bmatrix} 1 & 1 & 1 \\ 2\sin(\bar{\psi}_r(t)) & 2\sin(\bar{\psi}_r(t)+2\pi/3) & 2\sin(\bar{\psi}_r(t)+4\pi/3) \\ 2\cos(\bar{\psi}_r(t)) & 2\cos(\bar{\psi}_r(t)+2\pi/3) & 2\cos(\bar{\psi}_r(t)+4\pi/3) \end{bmatrix} \tag{11}$$

$$\mathbf{T}(\bar{\psi}_r(t)) = \begin{bmatrix} 1 & \sin(\bar{\psi}_r(t)) & \cos(\bar{\psi}_r(t)) \\ 1 & \sin(\bar{\psi}_r(t)+2\pi/3) & \cos(\bar{\psi}_r(t)+2\pi/3) \\ 1 & \sin(\bar{\psi}_r(t)+4\pi/3) & \cos(\bar{\psi}_r(t)+4\pi/3) \end{bmatrix} \tag{12}$$

The superscript nr denotes quantities expressed in non-rotating frame. After the transformation, these quantities have meanings in terms of rotor motion instead of individual blades. M^{nr}_{avg} represents average value of blade root bending moments and causes the rotor to bend as a cone. M^{nr}_{tilt} represents the moment from blades resulting in rotor tilt, and similarly M^{nr}_{yaw} is the moment in the yaw direction of rotor [17]. q^{nr}_1, q^{nr}_2, q^{nr}_3 are defined as rotor coning, rotor tip-path-plane fore-aft tilt and rotor tip-path-plane side-side tilt, respectively [18]. θ^{nr}_1 is the collective pitch command, while θ^{nr}_2 and θ^{nr}_3 are cyclic individual blade pitch commands.

The resulting state space matrices derived with the MBC transformation usually have significantly less variation due to rotor position compared to the matrices derived using rotating coordinate frames. Averaging these small amplitude variations in the periodic matrices generally yields acceptable results even with extreme wind conditions where the effects of periodicity are highest [11]. Controllers can be designed based on the resulting LTI approximation. A comparison of the LTI model used for control design and the periodic LTV and nonlinear system models are presented in Figure 2. Figure 2 shows the response of these models to a small perturbation in collective pitch input in rotating frame. The inputs and outputs of the LTI system is transformed through MBC and inverse MBC to obtain the system response in rotating frame. Note that there is excellent correlation among the responses except for the amplitude of the oscillations.

Since the LTI approximation is obtained with the input-output MBC transformations, these transformations must be implemented as a part of the controller on turbine. The LTI approximation of the periodic LTV system is shown in Figure 3 and the resulting periodic gain controller interconnection is shown in Figure 4. The inputs of the controller in the nonlinear simulations are $\Delta\Omega$, ΔM^{nr}_{avg}, M^{nr}_{tilt}, M^{nr}_{yaw} since these are the signals to be attenuated.

The MBC transformation is a function of the trim trajectory of rotor position. When implemented, the rotor position of the actual turbine will diverge from its trim trajectory due to varying wind conditions. Hence it is desired to use the actual rotor position, i.e. $\mathbf{T}(\psi_r(t))$ rather than $\bar{\mathbf{T}}(\psi_r(t))$, for the MBC transformation as discussed in the previous section. Further details of MBC can be found in [18], along with its application to numerical linearization data obtained through simulation codes.

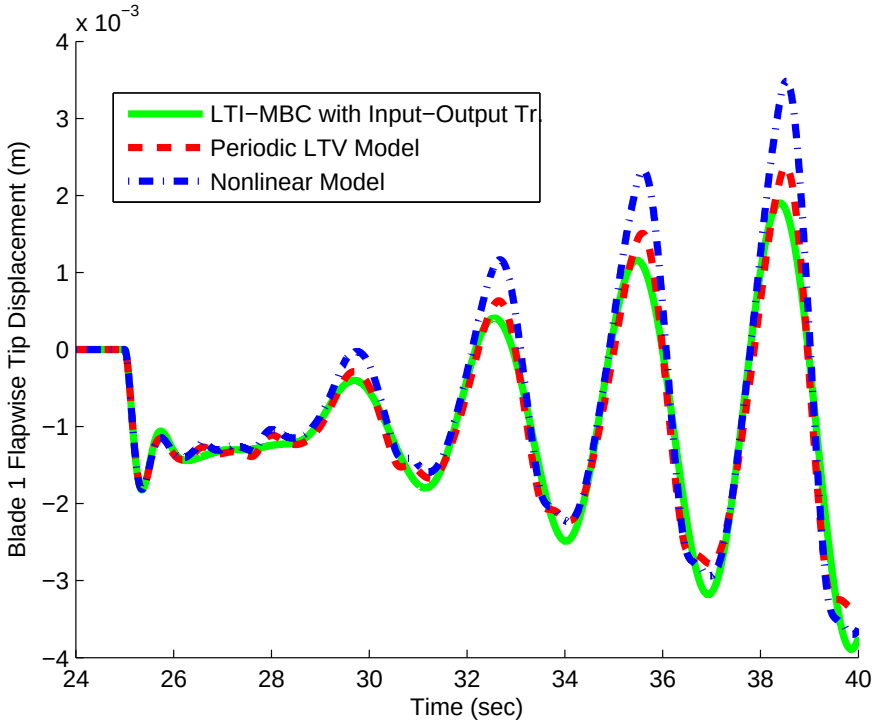

Figure 2: Comparison of LTI, LTV and Nonlinear System for small perturbations

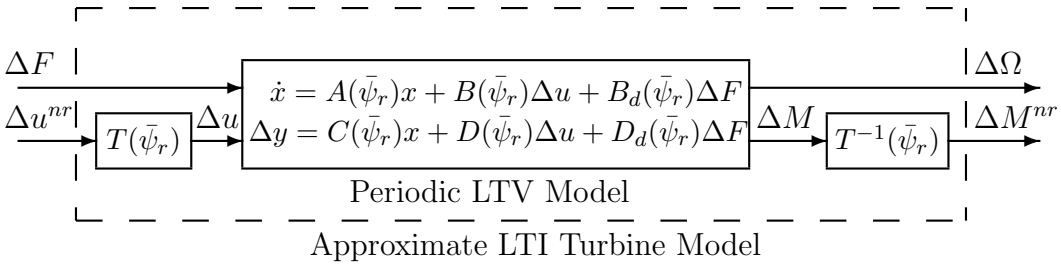

Figure 3: MBC application and Approximate LTI Turbine Model

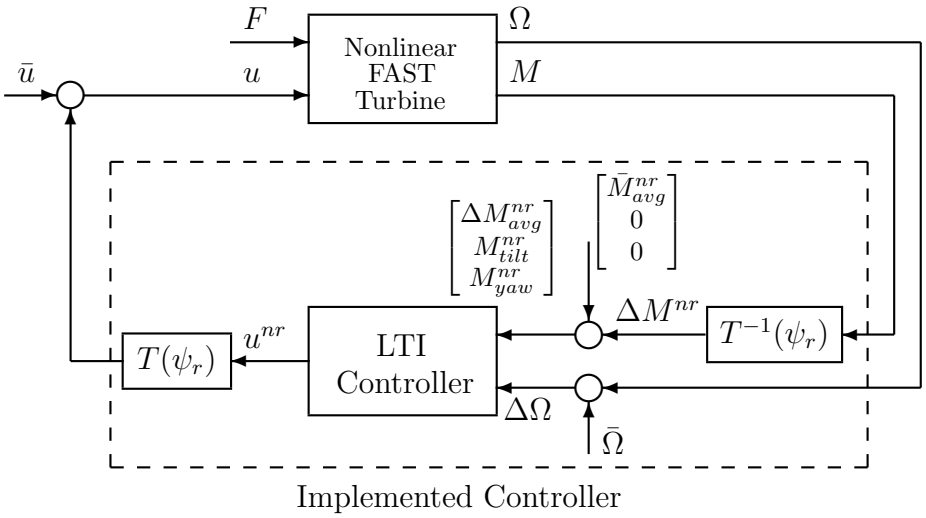

Figure 4: Controller Implementation on nonlinear system

3. Control Problem Formulation

Wind turbine control in Region 3 involves minimizing loads on the turbine structure and rotor speed deviations from the rated speed. A wind turbine is subject to turbulent wind disturbances, as well as persistent disturbances like gravity, tower shadow and wind shear. These persistent disturbances coupled with the rotor rotation result in a significant contribution to the $1p$ loads on the rotating structures and $3p$ loads on the non-rotating structures where np is defined as the n-th multiple of the rotor rotation frequency. Due to coupling of persistent disturbances and rotor rotation, a turbine operating under constant wind conditions still has oscillations in its trim trajectory (see Section 2.2). It is often desired to account for these persistent disturbances in addition to the standard load reduction problem into control problem formulation to further reduce loads on the turbine. Disturbance models are often used in literature for individual pitch control in order to attenuate effects of the disturbances on the turbine [7].

A two layered design procedure is used for regulating rotor speed and blade loads in this paper. The first layer consists of a rotor speed controller that uses rotor speed measurement to generate collective pitch commands. An individual pitch controller is designed for blade load reduction with the rotor speed controller implemented. The IPC takes M^{nr}_{avg}, M^{nr}_{tilt} and M^{nr}_{yaw} mea-

surements to generate cyclic pitch commands. To investigate the potential improvements that can be achieved through disturbance model augmentation as well as the potential stumbling blocks to implementation and refinement, two IPC are designed using H_∞ ([19],[20]) control design techniques. The first IPC design uses the disturbance model and the other baseline design does not. Both IPC designs share the same rotor speed controller. The reason for selecting a two layered design is to get similar rotor speed tracking and tower fatigue characteristics with different IPC controllers for a fair comparison of blade load reduction characteristics of the IPC algorithms. The decoupling of the control problem is not expected to impact the problem studied since the load reduction improvement by disturbance model augmentation is expected solely through cyclic pitch commands. On the other hand, it should be noted that the two layer approach does not take into account all the couplings in the system as well as the tradeoff between rotor speed tracking and load reduction problems. A single controller that accounts for all the couplings in the system might result in better overall performance.

For the H_∞ control problem, performance requirements for the turbine and controller are expressed in the frequency domain by selecting appropriate weights on system signals. The H_∞ control design approach used in this paper is built on the results of [3]. The system interconnection used for rotor speed control is shown in Figure 5.

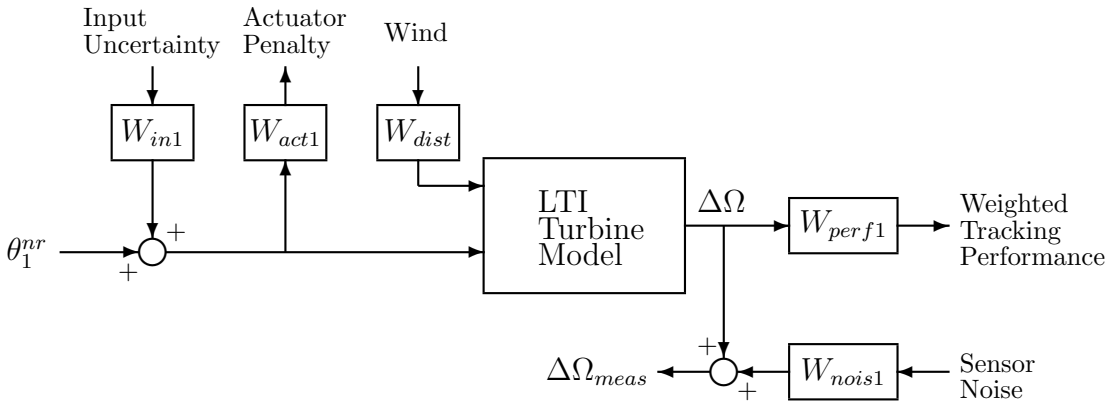

Figure 5: System Interconnection for H_∞ Rotor Speed Controller Design

W_{dist} models the characteristics of the expected turbulent wind disturbances. The wind conditions are assumed to consist of 5% turbulence inten-

sity on top of the steady wind conditions specified in Table 1. According to the The International Electrotechnical Commission (IEC) IEC-61400-1 standards [21, 22], 5% turbulence is defined as low turbulent wind conditions. Typically, class C wind turbines designed for low turbulence conditions must be able to operate in 13% wind turbulence, whereas class B and A wind turbines must withstand higher turbulence levels. Wind input data with 5% turbulence over steady wind conditions was generated using TurbSim [23], a stochastic, turbulent wind simulator. Since the input of the linear system is the deviation from steady wind conditions, the mean wind speed is subtracted from the raw data. The frequency spectrum is obtained using a Discrete Fourier Transform and its spectrum is overbounded with a transfer function to obtain W_{dist}. A Bode plot of W_{dist} and the frequency spectrum of the wind data are shown in Figure 6. The resulting W_{dist} is given in Eq. 13.

$$W_{dist}(s) = 0.25\frac{1/60s + 1}{1/4s + 1} \tag{13}$$

The rotor speed tracking problem involves minimizing the deviations from the rated rotor speed. This can be achieved by attenuating the gain from wind disturbances to rotor speed deviation output $\Delta\Omega$. The open loop Bode plot from wind disturbance to $\Delta\Omega$ is given in Figure 7. Figure 7 also contains closed loop results that will be discussed later. It can be seen that the poorest disturbance attenuation occurs at low frequencies and there is a valley at tower natural frequency. It is desired to improve the attenuation in this channel especially at low frequencies where the wind disturbance input has the highest gain. Since the system is rolling off quickly at frequencies beyond actuator bandwidth, a constant inverse weight $W_{perf1} = 1$ is chosen for W_{perf1} such that worse case deviation is 1 rpm. The main limitations on this objective are the coupling between tower fore-aft motion and the actuator bandwidth. Note that the controller should have a notch characteristic at the tower bending mode frequency to avoid exciting tower motion.

W_{act1} is the actuator penalty on the collective pitch command. The actuators on the turbine are considered to have pitch rate limitations of 0.1745 rad/s and bandwidth limitations of 10 rad/s. The actuator commands in rotating frame are transformed to nonrotating frame through $\theta^{nr} = \mathbf{T}^{-1}(\psi_r(t))\theta$ in time domain. In the frequency domain this corresponds to convolution. Hence it is non-trivial to precisely relate weights in rotating coordinates to nonrotating coordinates. Understanding the effect of an MBC transformation on the actuator signals is an open research topic that is not

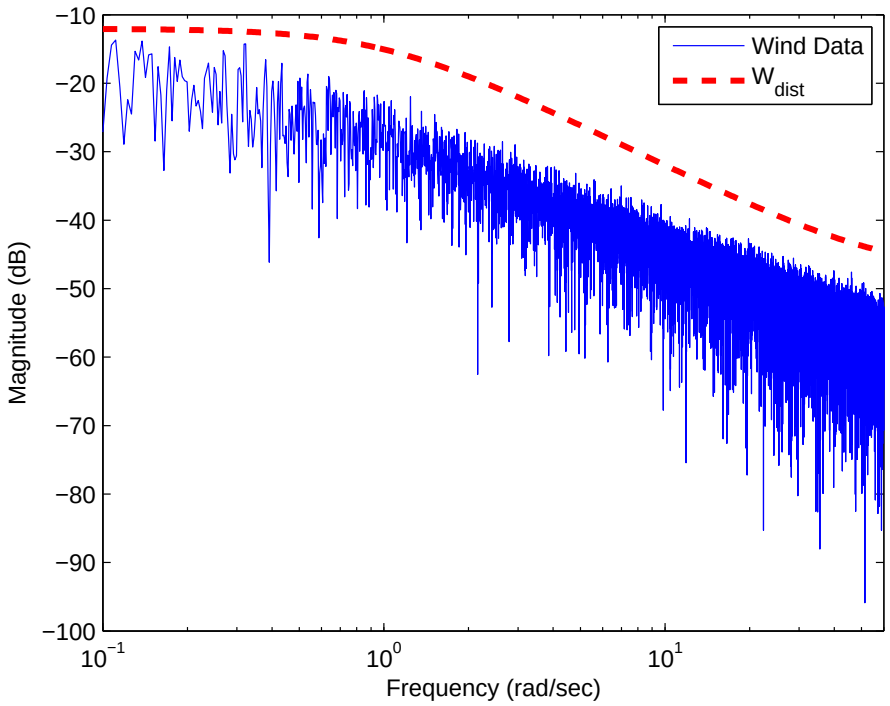

Figure 6: Frequency spectrum of 5% turbulent wind and W_{dist} input weight

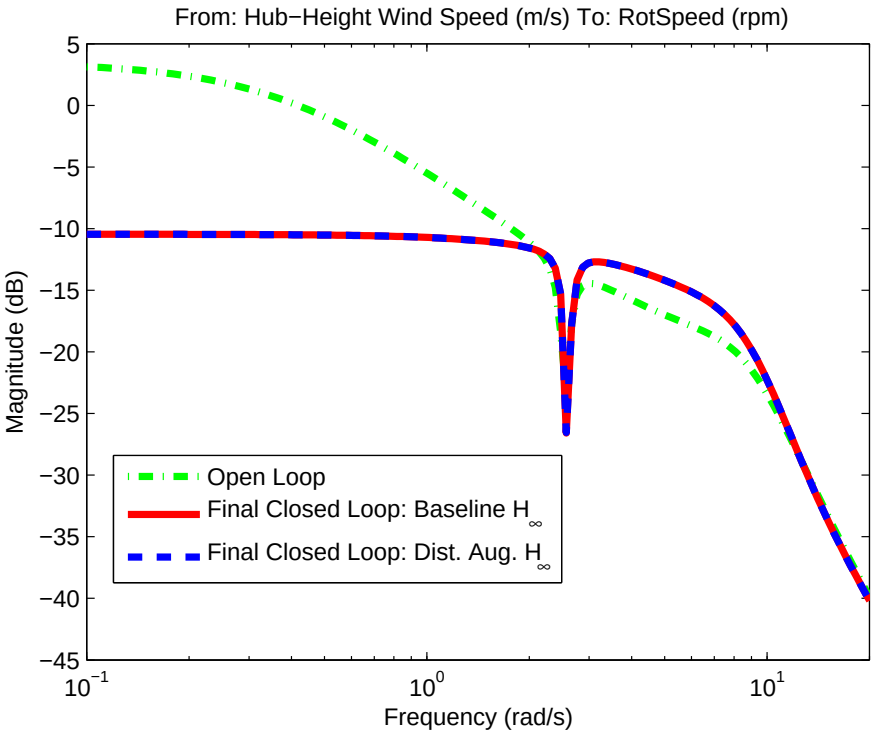

Figure 7: Bode Plots from Wind Disturbance to Rotor Speed Deviation

addressed in this research. For the scope of this study, a simpler but less precise approach was taken. A first order weight is chosen with the zero at $s = -10$ and the pole at $s = -80$ to penalize high frequency controller action. The gain of the weight is adjusted after a few iterations observing actuator signals in the nonlinear simulations. Rate limiters have been used to ensure that the actuator demands do not exceed physical actuator limits. The weight $W_{act1}(s)$ used in design is given in Eq. 14.

$$W_{act1}(s) = \frac{8}{\pi}\frac{1/10s + 1}{1/80s + 1} \tag{14}$$

An input uncertainty is added to the collective pitch command through the weight $W_{in1} = 0.01$ to model the difference between controller commands and actuator outputs. This value of W_{in1} typically corresponds to about 1% of the collective pitch commands expected by the controller. W_{nois1} was chosen to be 0.021. This approximately models noise with amplitude equal to 1% of rated rotor speed.

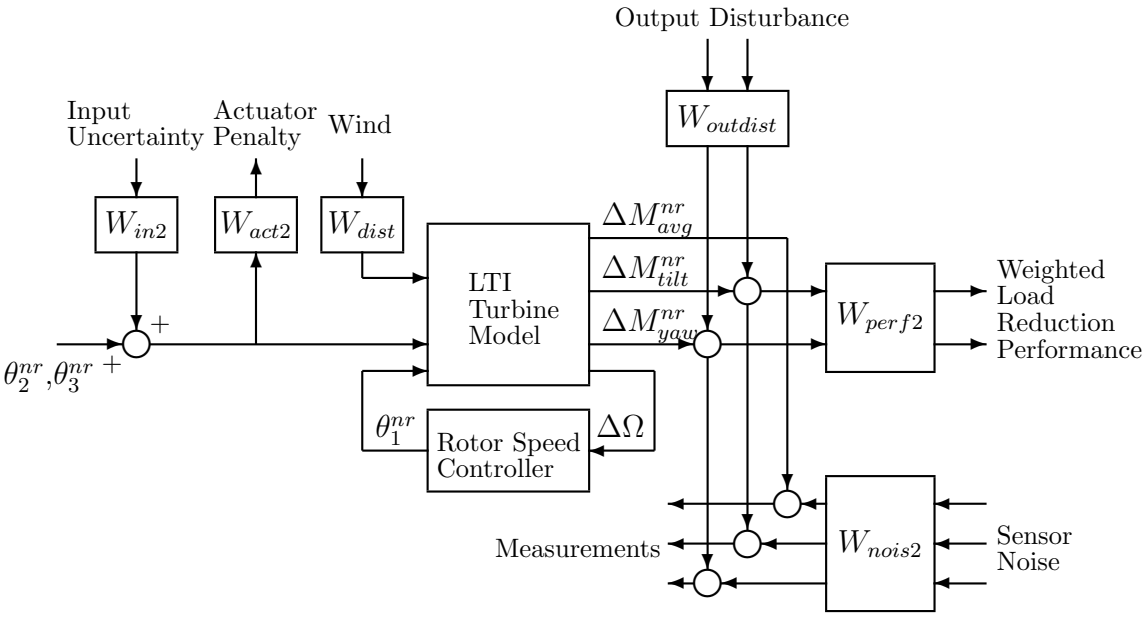

Figure 8: System Interconnection for H_∞ Individual Pitch Controller Design

The IPC design interconnection is presented in Figure 8. The wind turbine structural loads occur mostly at integer multiplies of the rotor frequency

due to rotation dynamics. Blade fatigue is dominated by the $1p$ dynamics of the turbine though the effects of the $2p$, $3p$ and $4p$ dynamics can be important to some extent where p is the rotor rotation frequency. These np rotation dynamics can be observed in $[M_1; M_2; M_3]$ blade bending loads as three sinusoidals with $\frac{2n\pi}{3} rad$ phase shift in between. In order to account for these loads observed in physical coordinates, the corresponding signals in nonrotating frame must be obtained through MBC transformation presented in Equation 15.

$$\begin{bmatrix} M^{nr}_{avg} \\ M^{nr}_{tilt} \\ M^{nr}_{yaw} \end{bmatrix} = \mathbf{T}^{-1}(\bar{\psi}_r(t)) \begin{bmatrix} sin(npt) \\ sin(n(pt + \frac{2\pi}{3})) \\ sin(n(pt + \frac{4\pi}{3})) \end{bmatrix} \tag{15}$$

Transformation of some of the important rotation dynamics are summarized in Table 2. The superscript nr is used when frequencies and quantities expressed in nonrotating frame are referred. For instance, in order to reduce loads caused by $1p$ dynamics of the system, $0p^{nr}$ (DC component) of M^{nr}_{tilt} and M^{nr}_{yaw} must be penalized. For reduction of loads caused by $2p$ and $4p$ dynamics of rotation, the $3p^{nr}$ of M^{nr}_{tilt} and M^{nr}_{yaw} must be penalized. The traditional IPC problem usually ignores the M^{nr}_{avg} channel since individual pitch control has limited effect on this channel. Hence it is seen that loads caused by $3p$, $6p$, $9p$... dynamics are not accounted when M^{nr}_{avg} is neglected. It should be noted that Table 2 only summarizes transformation of wind turbine rotating dynamics which consist of three sinusoidals at np frequency with $\frac{2n\pi}{3}$ phase shifts; and not the transformation of any arbitrary three sinusoidals at np frequency.

Table 2: Transformation of System Dynamics through MBC

Rotating Frame Dynamics	Nonrotating Frame
$1p$, separated by $\frac{2\pi}{3} rad$	$0p^{nr}$ (DC) @ M^{nr}_{tilt} and M^{nr}_{yaw}
$2p$, separated by $\frac{4\pi}{3} rad$	$3p^{nr}$ @ M^{nr}_{tilt} and M^{nr}_{yaw}
$3p$, separated by $0rad$	$3p^{nr}$ @ M^{nr}_{avg}
$4p$, separated by $\frac{2\pi}{3} rad$	$3p^{nr}$ @ M^{nr}_{tilt} and M^{nr}_{yaw}
$5p$, separated by $\frac{4\pi}{3} rad$	$6p^{nr}$ @ M^{nr}_{tilt} and M^{nr}_{yaw}
$6p$, separated by $0rad$	$6p^{nr}$ @ M^{nr}_{avg}
$7p$, separated by $\frac{2\pi}{3} rad$	$6p^{nr}$ @ M^{nr}_{tilt} and M^{nr}_{yaw}

The block diagonal performance weight W_{perf2} contains two first order weights for yaw and tilt moments to reflect the performance demands of reducing loads at $0p^{nr}$ and low frequencies in nonrotating frame. This represents the demand of reducing $1p$ loads as well as other low frequency components of the blade loads caused by turbulent wind conditions in rotating frame. Velocity and acceleration limits on the actuators play a large role in this objective, and commonly compensation on modes beyond the $3p$ or $4p$ frequencies are avoided to prevent exciting blade bending modes and other high-order system dynamics. It should be noted that the choice of performance weights do not penalize the $3p^{nr}$ frequency. Hence it is expected that the controller will not provide significant improvements for $2p$ and $4p$ loads. The weight $W_{perf2}(s)$ used in design is given in Eq. 16.

$$W_{perf2} = 0.032 \begin{bmatrix} \frac{1}{1/0.05s+1} & 0 \\ 0 & \frac{1}{1/0.05s+1} \end{bmatrix} \tag{16}$$

W_{nois2} is chosen as a block diagonal constant weight to incorporate the noise on blade bending moment sensors transformed to nonrotating frame. Its gain is chosen to be 1% of their values at trim operating condition. W_{act2} is chosen as a first order weight for the actuator penalty on cyclic pitch commands to limit the bandwidth of the compensation. The values of W_{nois2} and W_{act2} are given in Equations 17 and 18 respectively. $W_{in2} = \begin{bmatrix} 0.01 & 0 \\ 0 & 0.01 \end{bmatrix}$ is the input uncertainty on cyclic pitch commands. W_{in2} is included to model the difference between actuator outputs and controller commands.

$$W_{nois2} = \begin{bmatrix} 6 & 0 & 0 \\ 0 & 1.5 & 0 \\ 0 & 0 & 1.5 \end{bmatrix} \tag{17}$$

$$W_{act2}(s) = \frac{3}{\pi} \begin{bmatrix} \frac{1/10s+1}{1/80s+1} & 0 \\ 0 & \frac{1/10s+1}{1/80s+1} \end{bmatrix} \tag{18}$$

The output disturbances are modeled based on the trim trajectory of the system. The trajectories of the system outputs ($\bar{y}$), expressed in the original (rotating) coordinate frame, are obtained with a simulation under steady wind conditions. These trim trajectories include the effects of all persistent disturbances acting on the turbine. To incorporate this information into the

controller design procedure in the non-rotating frame, the MBC transformation is applied on $\bar{y}(t)$ to obtain $\bar{y}^{nr}(t)$ in the nonrotating frame. Here only $\bar{M}^{nr}_{tilt}$ and $\bar{M}^{nr}_{yaw}$ are modeled as output disturbances to represent the moments in tilt and yaw direction. The variations observed in the rotor speed trajectory are negligible due to large inertia or the rotor. Similarly, $\bar{M}^{nr}_{avg}$ has small variations with respect to rotor position and is not included. A Discrete Fourier Transform of $\bar{M}^{nr}_{tilt}$ and $\bar{M}^{nr}_{yaw}$ is obtained and these are over-bounded with transfer functions $G_1(s) = \dfrac{132.1s^2 + 5670s + 5478}{1000s^3 + 86.87s^2 + 41480s + 41.48}$ and $G_2(s) = \dfrac{-129.8s^2 - 5572s - 5383}{1000s^3 + 86.87s^2 + 41480s + 41.48}$ respectively. Then the output disturbance model is chosen as $W_{outdist1}(s) = \gamma \begin{bmatrix} G_1(s) & 0 \\ 0 & G_2(s) \end{bmatrix}$ with $\gamma = 6$ to ensure that the H_∞ optimization is focused on the output disturbances. A second disturbance model is obtained by simulating the system with 5% turbulence and then following the same MBC and Discrete Fourier Transformation procedure. This disturbance model has very similar peaks at the $0p^{nr}$ and $3p^{nr}$ frequencies but with higher gains at frequencies in between. This disturbance is modeled with $G_{1t}(s) = \dfrac{132.1s^2 + 5670s + 5478}{25s^3 + 108.3s^2 + 1041s + 41.48}$ and $G_{2t}(s) = \dfrac{-129.8s^2 - 5572s - 5383}{25s^3 + 108.3s^2 + 1041s + 41.48}$ respectively. This second model is given by Then the output disturbance model is chosen as $W_{outdist2}(s) = \gamma \begin{bmatrix} G_{1t}(s) & 0 \\ 0 & G_{2t}(s) \end{bmatrix}$ with $\gamma = 12$.

The disturbance models used for M^{nr}_{tilt} and M^{nr}_{yaw} channels obtained using steady wind conditions are shown in Figure 9. The disturbance models obtained with the turbulent wind conditions are shown in Figure 10. In the H_∞ framework, these disturbance models are driven by bounded L_2 signals. A scalar signal $u(t)$ is in L_2 if $||u||_2 < \infty$ where the 2-norm of $u(t)$ is defined as:

$$||u||_2 := \left(\int_0^{+\infty} u(t)^2 dt \right)^{1/2}$$

If $\exists M, T < \infty$ such that $|u(t)| < M \ \forall t \in [0, T]$ and $u(t) = 0$ for $t > T$, then $u(t) \in L_2$. Hence bounded L_2 signals can provide a reasonable representation for wind and persistent disturbances encountered in any finite-time experiment. In other words, any bounded wind or persistent disturbance signal that can be seen in any finite time T can be represented by L_2 signals.

Output disturbances were used to model the effects of persistent disturbances for several reasons. First, the trim trajectory combines several effects, e.g. tower shadow, that can be difficult to model as input to the linear system. Second, this approach results in a simpler controller design procedure in the sense that fewer weights need to be chosen. A single weight can be used to model the cumulative effect of several disturbances.

The interconnection presented in Figure 5 is used to design a rotor speed controller. The disturbance augmented H_∞ individual pitch controllers were designed using the interconnection in Figure 8 with two different disturbance models. The baseline H_∞ IPC was designed using the same interconnection but without the output disturbance model. The resulting H_∞ norm of the closed-loop interconnection for both IPC designs were less than 1 which means performance objectives specified as defined by the weights are achieved.

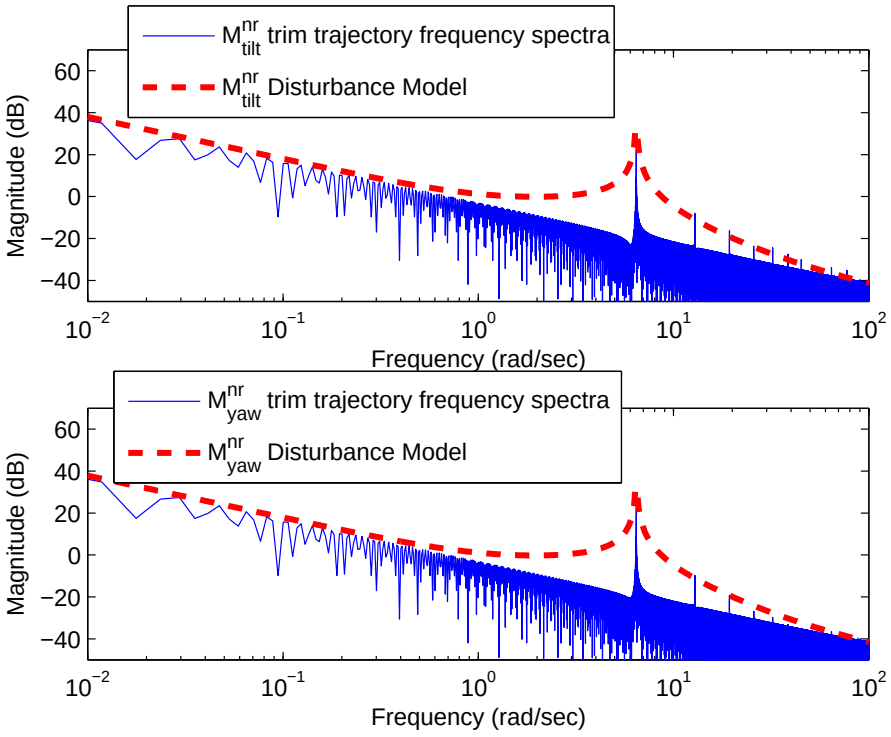

Figure 9: Frequency spectrum of output trim trajectories and Bode plots of disturbance models

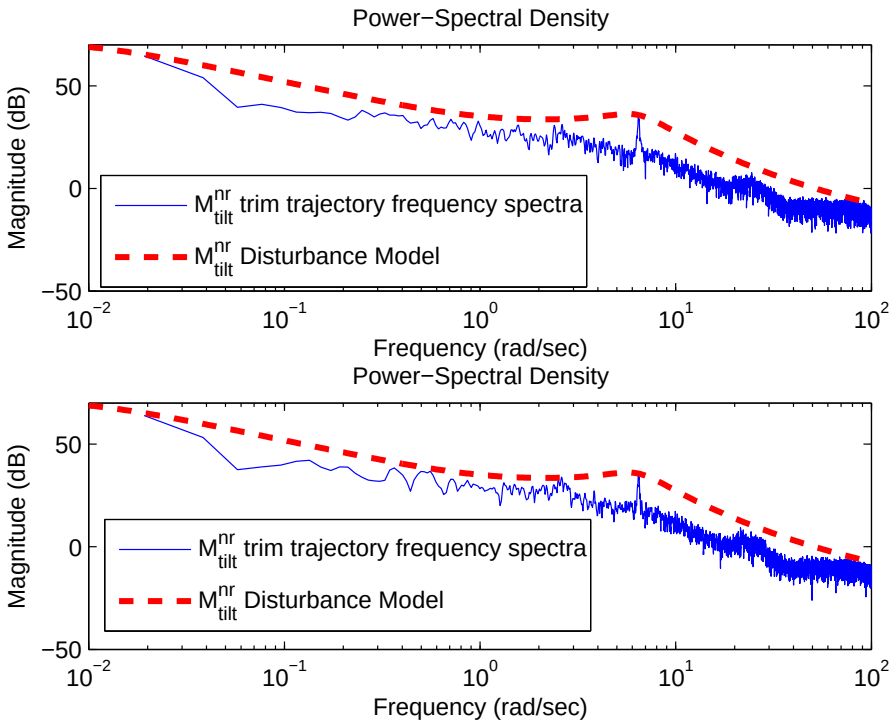

Figure 10: Frequency spectrum of output trajectories under 5% turbulence and Bode plots of disturbance models

4. Results

4.1. Linear Frequency-domain Analysis

Two IPC controllers obtained using different disturbance models yielded similar performance. Hence the rest of the paper only compares the baseline controller against the disturbance augmented controller using the disturbance model obtained from the nonlinear system's trim trajectory under steady wind conditions. Table 3 lists the frequencies of wind turbine modes of interest that are used in the analysis.

Table 3: Frequencies of System Modes of Interest

Description	Value
Rotor frequency (1p frequency)	2.15 rad/s
Tower bending mode frequency	2.55 rad/s

Figure 7 shows open and closed-loop Bode plots from the wind disturbance to rotor speed deviation output. The closed-loop Bode plots show notably less gain at lower frequencies where the turbulent wind inputs have their highest magnitude. Both controllers have similar performance including a notch characteristic at the tower natural frequency. This notch characteristic is important to avoid exciting the tower bending mode.

Figure 11 shows the Bode plot from wind disturbance to M^{nr}_{tilt}. Here the baseline controller shows approximately 85 dB improvement at low frequencies compared with the disturbance augmented controller 92 dB improvement over the open-loop performance at low frequencies. Since the most dominant blade loads caused by $1p$ dynamics of the system get mapped to DC frequency after MBC transformation, both controllers are expected to achieve significant load reduction. The disturbance augmented controller shows slightly lower attenuation in the frequency range of 0.1-2.5 rad/s while showing a small improvement around $3p^{nr}$ frequency of 6.45 rad/s. This is due to low performance penalty at $3p^{nr}$ by W_{perf2}.

For M^{nr}_{yaw}, the baseline controller shows about 86 dB improvement and the disturbance augmented controller shows about 88 dB improvement at low frequencies (Figure 12). Characteristics of the controllers in this channel are identical to M^{nr}_{tilt} channel including the small improvement at the $3p^{nr}$ frequency by the disturbance augmented controller. These results indicate

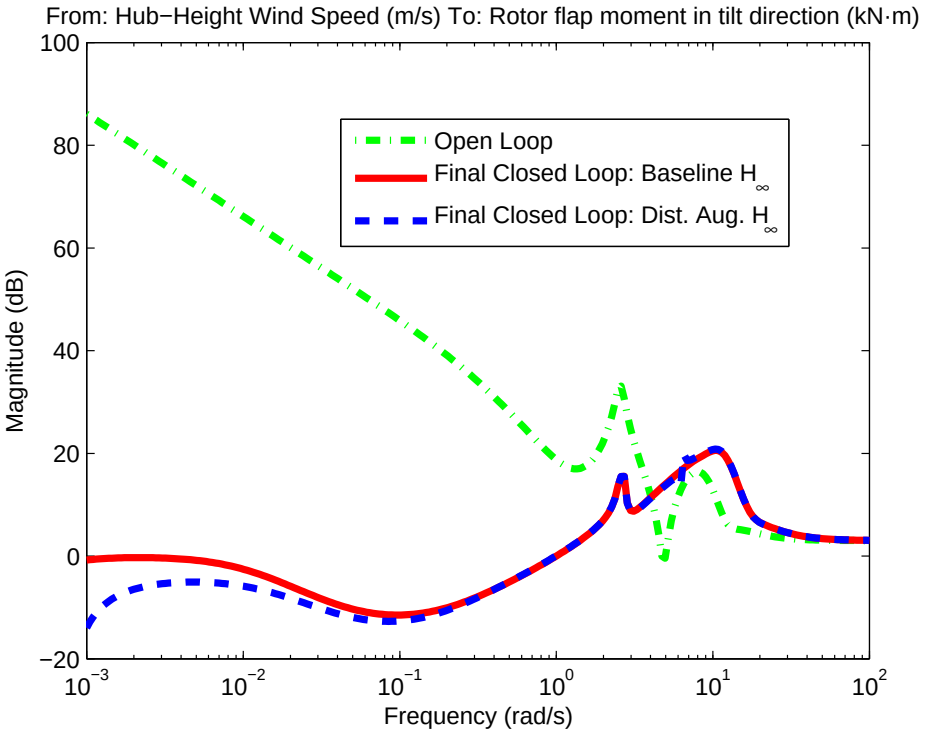

Figure 11: Bode Plots from Wind Disturbance to M_{tilt}^{nr}

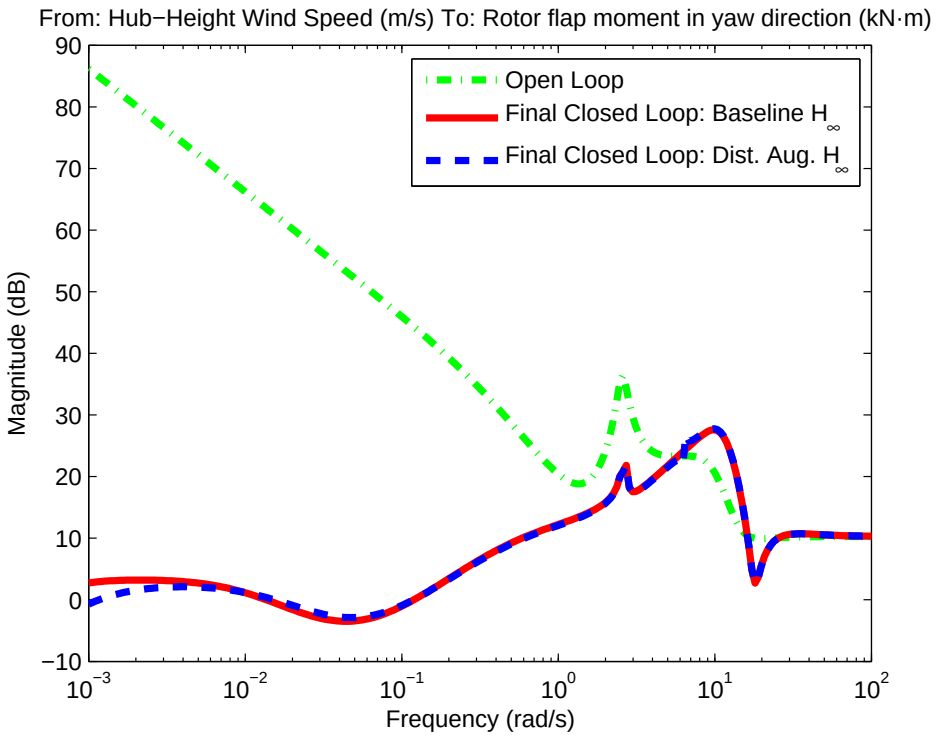

Figure 12: Bode Plots from Wind Disturbance to M_{yaw}^{nr}

both controllers are expected to yield important fatigue reduction in yaw channel.

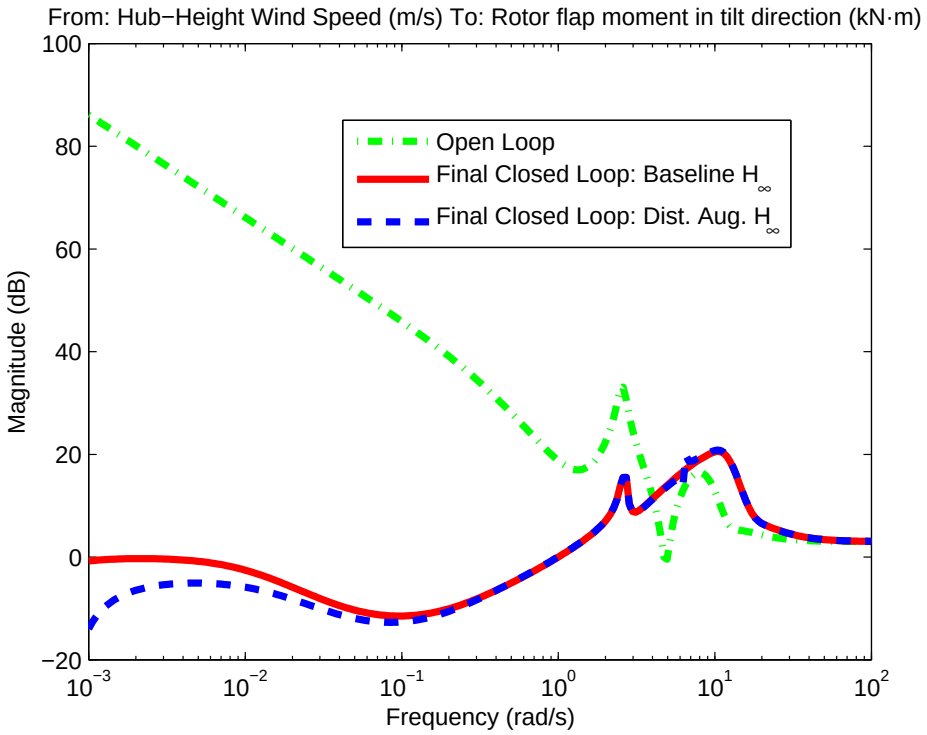

Figure 13: Open and Closed Loop Bode Plots for disturbance on M^{nr}_{tilt} to M^{nr}_{tilt}

The disturbance augmented controller interconnection presented in Figure 8 included two additional disturbance inputs that drive the M^{nr}_{tilt} and M^{nr}_{yaw} outputs independently. The total disturbance rejection characteristics of individual pitch controllers depend on rejection of these output disturbances affecting M^{nr}_{tilt} and M^{nr}_{yaw} channels as well as rejection of wind disturbances. The Bode plot from disturbance acting on M^{nr}_{tilt} to M^{nr}_{tilt} output is given in Figure 13 and the yaw channel disturbance is given in Figure 14. The baseline controller shows about 45 dB improvement at low frequencies with negligible effect at $3p^{nr}$ mode in both channels. The disturbance augmented controller achieves an improvement of 60 dB improvement at low frequencies in nonrotating frame and also a limited improvement at $3p^{nr}$ dynamics just about 3 dB attenuation for both channels.

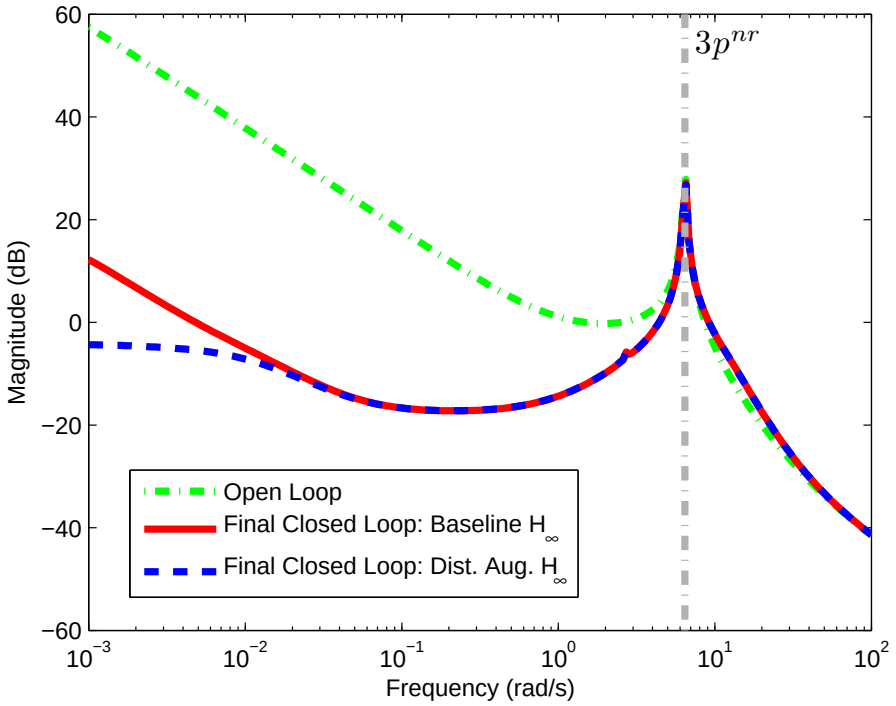

Figure 14: Open and Closed Loop Bode Plots for disturbance on M^{nr}_{yaw} to M^{nr}_{yaw}

It is not straightforward to quantify the combined effect of linear disturbance rejection results on the nonlinear system response for arbitrary wind inputs. For steady wind conditions, the disturbance augmented controller is expected to cancel out $1p$ rotor dynamics better in the rotating frame, while $2p$ and $4p$ dynamics are expected to show slight improvement. If increased attenuation of blade oscillations is desired in steady wind conditions, the performance weights on M^{nr}_{tilt} and M^{nr}_{yaw} can be increased at $3p^{nr}$ frequency. This would improve attenuation at $2p$ and $4p$ frequencies.

4.2. Nonlinear Time-domain Wind Turbine Simulations

The rotor speed and individual pitch controllers are simulated in the high order, 15 DOF nonlinear turbine model in FAST. The yaw dynamics are excluded from the nonlinear model as discussed in Section 2.1. The simulations are conducted with steady wind conditions given in Table 1, and the addition of 1% and 5% turbulence to the steady winds. These turbulence levels are typically considered as low turbulence wind conditions by national and international wind turbine design standards. Dynamic inflow and dynamic stall effects are included in aerodynamic force calculations. The hub-height uniform wind component of the turbulent wind is given in Figure 15.

Blade fatigue characteristics are evaluated by comparing blade damage equivalent loads (DEL) using MCrunch [24], assuming a S-N curve (cyclic stress (S) versus number of cycles to failure (N)) slope of 10. Rotor speed tracking error is compared by calculating root-mean-square (RMS) deviations from the rated rotor speed using the time domain simulation results. The actuator usage is compared in time domain using the maximum value of pitch rate and RMS value of pitch rate of blades. The results are summarized in Table 4. Tower fatigue in fore-aft direction is also calculated to validate that the control law does not adversely affect the tower loads.

The power spectral density (PSD) obtained using the p-Welch algorithm of root bending moment of Blade 1 is presented in Figure 16 for steady wind conditions. Data sets for each simulation are divided into 12 segments with 50% overlap and a Hamming window is used as the window function. Figure 16 shows that under steady wind conditions most of the blade loading occurs at multiples of the rotor frequency, i.e. $1p$,$2p$,$3p$,$4p$, and at the tower natural frequency. The disturbance augmented controller almost completely cancels out the $1p$ component of the load as well as improving results at $2p$ and $4p$ significantly. This agrees well with the choice of performance weight W_{perf2} which was heavily penalizing $0p^{nr}$ in nonrotating frame. Even though

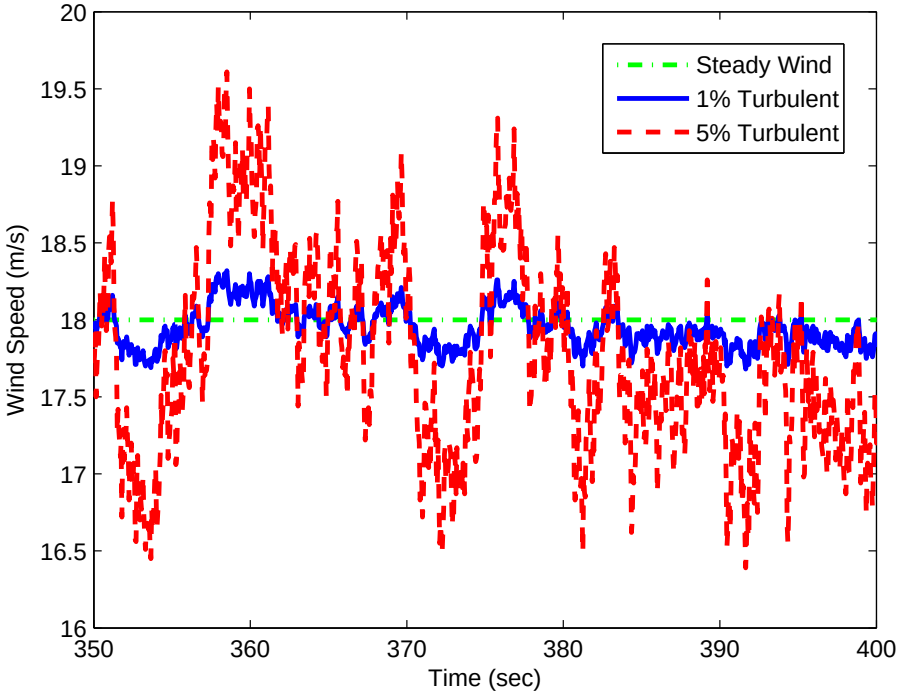

Figure 15: Hub-height wind disturbances used in simulations

Table 4: Controller Performance Comparison for Nonlinear Simulations

Description	Baseline H_∞	Dist. Aug. H_∞
Steady Wind		
Blade root flapwise DEL	38.52	32.98
Tower fore-aft bending DEL	130	129.2
RMS Rotor Speed Error (rad/s)	0.033	0.033
RMS Pitch Rate (rad/s)	0.036	0.036
Max Pitch Rate (rad/s)	0.063	0.063
1% Turbulent Wind		
Blade root flapwise DEL	100.2	98.70
Tower fore-aft bending DEL	538.8	537.9
RMS Rotor Speed Error (rad/s)	0.059	0.059
RMS Pitch Rate (rad/s)	0.037	0.037
Max Pitch Rate (rad/s)	0.078	0.079
5% Turbulent Wind		
Blade root flapwise DEL	452.7	452.5
Tower fore-aft bending DEL	2687	2689
RMS Rotor Speed Error (rad/s)	0.265	0.265
RMS Pitch Rate (rad/s)	0.042	0.042
Max Pitch Rate (rad/s)	0.146	0.156

the W_{perf2} did not have a significant gain at $3p^{nr}$, the disturbance model has included $3p^{nr}$ components of the persistent disturbances. Hence controller shows some improvements at $3p^{nr}$ mode in nonrotating frame as well, which carries loads from $2p$ and $4p$ dynamics of the rotation as summarized in Table 2. If further reduction of loads at these frequencies are desired, the gain of the W_{perf2} can be modified to have a higher gain at $3p^{nr}$ frequency. The PSD of only the speed-regulated turbine (no IPC) is not included here since it carried a substantially large $1p$ and $2p$ components that rendered all other details of the plot indistinguishable. The peaks of the PSD of the only speed regulated turbine occurred at 500000 for $1p$ and 2100 for $2p$ frequency compared to the values observed in Figure 16. In steady wind, the turbine with speed control only (no IPC) achieved a DEL of 463.4. Overall both controllers show substantial load reduction compared to the speed control only but the disturbance augmented design performs slightly better.

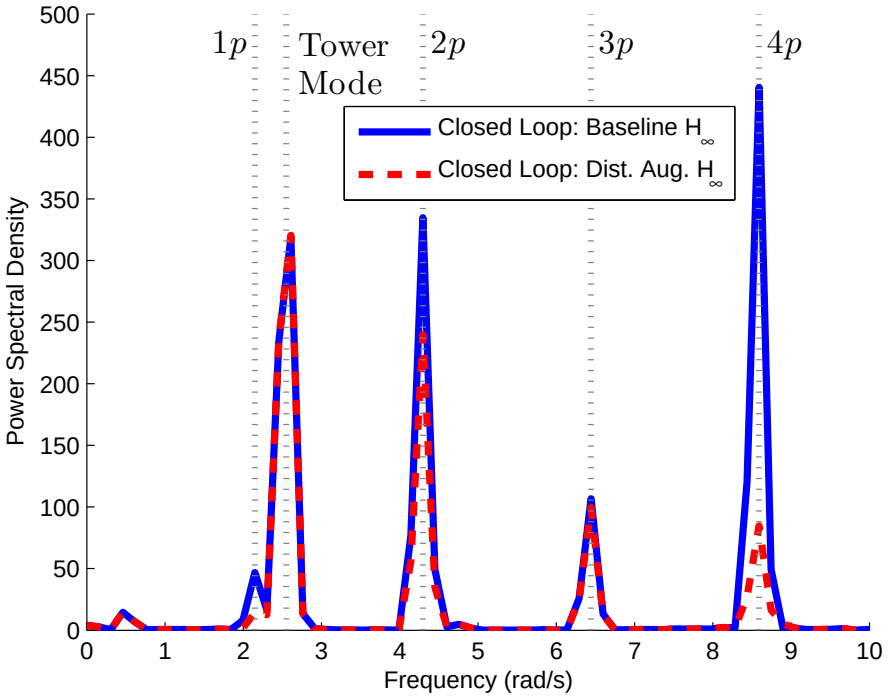

Figure 16: PSD of Blade 1 Root Bending Moment response under steady wind conditions

The PSD of Blade 1 root bending moment due to 1% turbulent wind

conditions is presented in Figure 17. Figure 17 shows that with the inclusion of 1% turbulence, the peaks of the PSD no longer just occur at multiples of rotor frequency but also at frequencies where wind turbulence carries energy. Improvements by the disturbance augmented controller are still distinguishable at multiples at rotor frequencies. But the percentage-wise improvement is decreased due to increasing contribution to fatigue from M_{avg}^{nr} channel as well as loads at a wider frequency band in M_{yaw}^{nr} and M_{tilt}^{nr}.

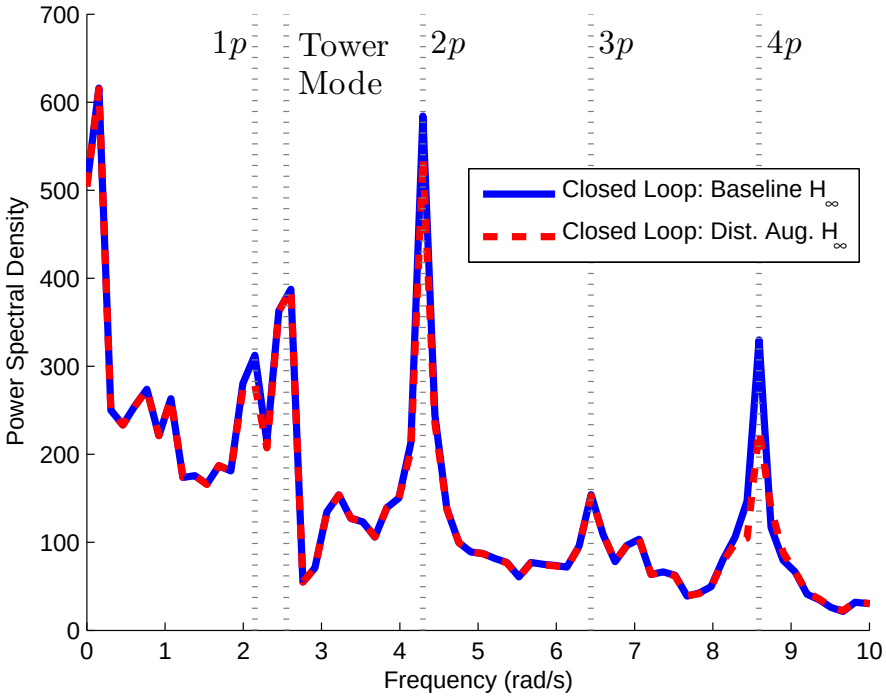

Figure 17: PSD of Blade 1 Root Bending Moment response under 1% turbulent wind

The PSD of Blade 1 root bending moment under 5% turbulence is presented in Figure 18. This plot also includes results from the IPC controller obtained using disturbance model from 5% turbulent wind conditions and this controller achieves a DEL of 452.6. Both disturbance augmented controllers show a very limited DEL improvement. Improvements by both disturbance augmented controllers are no longer distinguishable from the PSD plot. The effects of wind turbulence are more pronounced and most of the blade loads are occurring at the low frequency range between 0 rad/s and 1

rad/s.

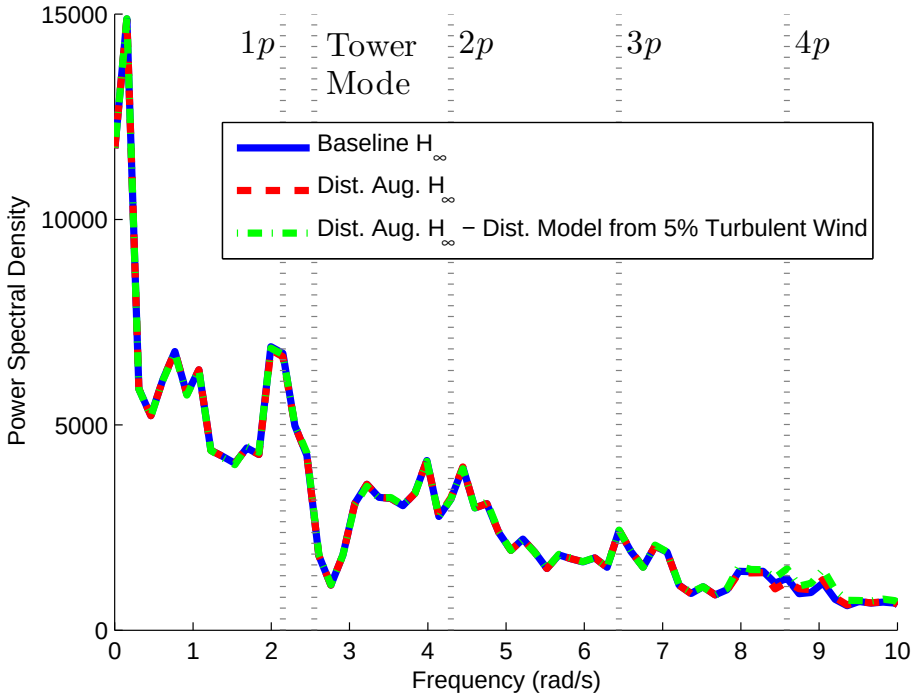

Figure 18: PSD of Blade 1 Root Bending Moment response under 5% turbulent wind

The PSD of the M^{nr}_{avg} and M^{nr}_{tilt} channels under steady, 1% turbulent and 5% turbulent wind are given in Figure 19 and 20, respectively. Figure 20 shows that the asymmetrical loads on rotor are spread over a wider frequency range in M^{nr}_{tilt} channel. Figure 19 shows that the ratio of the loads in M^{nr}_{avg} channel to the loads in M^{nr}_{tilt} channel increases rapidly. In steady winds, the majority of the blade loads occur in the M^{nr}_{tilt} and M^{nr}_{yaw} channels. However, the loads in the M^{nr}_{avg} channel dominate the blade loads under 5% turbulent wind conditions. Hence any improvement obtained in M^{nr}_{tilt} and M^{nr}_{yaw} channels becomes less significant as the bending moment of Blade 1 is $M_1 = M^{nr}_{avg} + sin(\psi_r(t))M^{nr}_{tilt} + cos(\psi_r(t))M^{nr}_{yaw}$ from Eqs. 10 and 12. The disturbance augmented design achieves load reduction improvements only at the multiples of the rotor frequency in the M^{nr}_{tilt} and M^{nr}_{yaw} channels. The effect of disturbance augementation diminishes in turbulent conditions because the loads in the M^{nr}_{avg} channel begin to dominate the loads. Moreover,

this phenomena even occurs at low turbulence levels such as 1% which is typically lower than the turbulence levels observed at wind farms.

Finally it is worth noting that the controllers designed in this paper are periodic since they must be implemented with the MBC transformations at the controller inputs and outputs. Thus LTI turbine models obtained using MBC are rich enough to capture periodic turbine dynamics. An alternative LTI turbine model can be obtained by simply averaging linearizations obtained at different rotor positions. An LTI model obtained via this averaging method will lose most of the periodic dynamic effects and thus will be of lower model fidelity. It is possible that disturbance augmentation might lead to more significant reductions in blade loads compared to controllers without disturbance models if the controllers are designed on averaged LTI models.

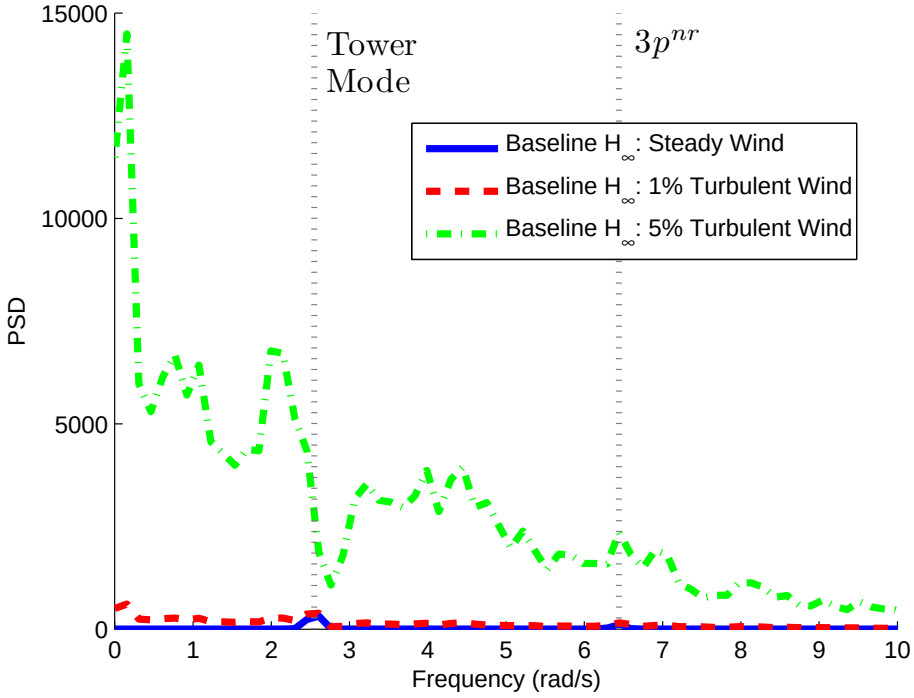

Figure 19: The PSD of M_{avg} Channel

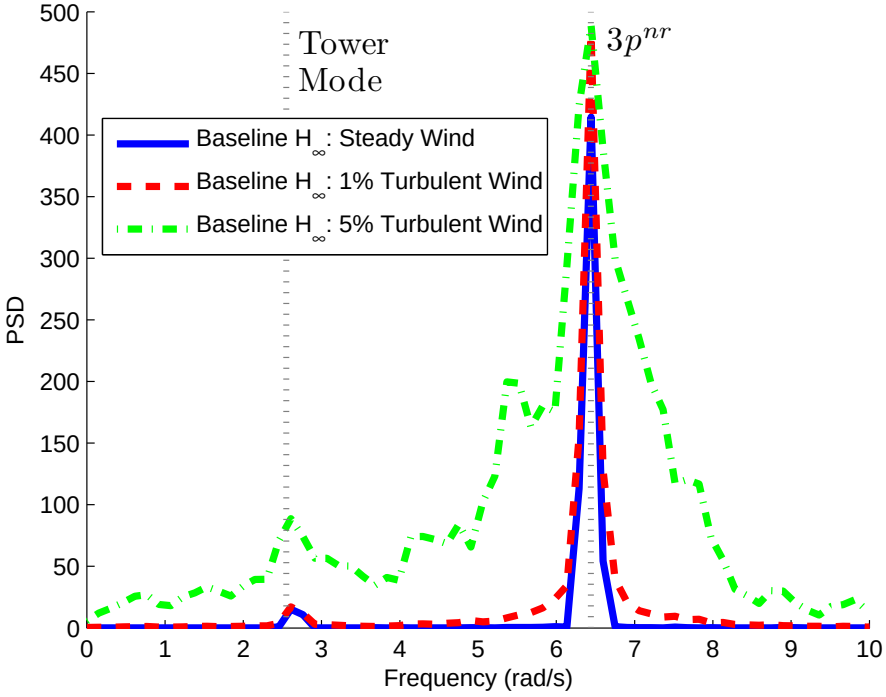

Figure 20: The PSD of M_{tilt} Channel

5. Conclusions

This paper investigates the effects of disturbance model augmentation for individual pitch control design. In the literature, disturbance augmentation is used for accommodating persistent disturbances causing loads at the multiples of the rotor frequency. A baseline H_∞ controller was designed for individual pitch control and compared to a second controller that incorporates a disturbance model into design procedure. The effects of the added disturbance model were investigated through linear analysis as well as nonlinear simulations presented in time and frequency domains. Results show that augmenting the disturbance model yields performance improvements at steady and low turbulent wind conditions. Though both controllers yield similar performance characteristics as the turbulence increases. This is due to the high collective loading of the blades caused by turbulence, which is not addressed by the IPC algorithms. In addition, as energy from the turbulent wind conditions spreads through a broader frequency spectrum, improvements obtained at multiples of the rotor frequency are less important. Hence disturbance model augmentation may not yield expected performance improvements under turbulent wind conditions.

6. Acknowledgements

This work was supported by the University of Minnesota Institute on the Environment, IREE Grant No. RS-0039-09, the US Department of Energy Contract No. DE-EE0002980 and the US National Science Foundation under Grant No. NSF-CNS-0931931. Any opinions, findings, and conclusions or recommendations expressed in this material are those of the author(s) and do not necessarily reflect the views of the University of Minnesota, Department of Energy or National Science Foundation.

References

[1] E. A. Bossanyi, The design of closed loop controllers for wind turbines, Wind Energy 3 (3) (2000) 149–163.

[2] E. A. Bossanyi, Individual blade pitch control for load reduction, Wind Energy 6 (2) (2003) 119–128.

[3] M. Geyler, P. Caselitz, Robust multivariable pitch control design for load reduction on large wind turbines, Journal of Solar Energy Engineering 130 (3) (2008) 031014.

[4] C. D. Johnson, Theory of disturbance-accommodating controllers, Control and Dynamic Systems 12 (1976) 387–489.

[5] K. A. Stol, M. J. Balas, Periodic disturbance accommodating control for blade load mitigation in wind turbines, Journal of Solar Energy Engineering 125 (4) (2003) 379–385.

[6] A. D. Wright, M. J. Balas, Design of controls to attenuate loads in the controls advanced research turbine, Journal of Solar Energy Engineering 126 (4) (2004) 1083–1091.

[7] J. H. Laks, L. Y. Pao, A. D. Wright, Control of wind turbines: Past, present, and future, in: Proceedings of American Control Conference, St. Louis, Missouri, 2009, pp. 2096–2103.

[8] K. A. Stol, Dynamics modeling and periodic control of horizontal-axis wind turbines, Ph.D. thesis, University of Colorado at Boulder, Boulder, Colorado (2001).

[9] W. Johnson, Helicopter Theory, 1st Edition, Princeton University Press, 1980.

[10] R. Coleman, A. Feingold, Theory of self-excited mechanical oscillations of helicopter rotors with hinged blades, Tech. rep., NASA (1958).

[11] K. A. Stol, H.-G. Moll, G. Bir, H. Namik, A comparison of multi-blade coordinate transformation and direct periodic techniques for wind turbine control design, in: Proceedings of the 47th AIAA/ASME, Orlando, Florida, 2009, pp. AIAA–2009–479.

[12] J. Laks, L. Pao, A. Wright, Combined Feed-forward/Feedback Control of Wind Turbines to Reduce Blade Flap Bending Moments, in: 47th AIAA Aerospace Sciences Meeting, 2009, pp. AIAA–2009–687.

[13] J. Laks, L. Y. Pao, E. Simley, A. Wright, N. Kelley, Model predictive control using preview measurements from lidar, in: 49th AIAA Aerospace Sciences Meeting, 2011, pp. AIAA–2011–813.

[14] J. M. Jonkman, J. M. L. Buhl, FAST User's Guide, National Renewable Energy Laboratory, Golden, Colorado (2005).

[15] A. C. Hansen, Users Guide to the Wind Turbine Dynamics Computer Programs YawDyn and AeroDyn for ADAMS version 11.0, Mech. Eng. Dept. University of Utah, Golden, Colorado (1998).

[16] K. Stol, M. Balas, Full-state feedback control of a variable-speed wind turbine: A comparison of periodic and constant gains, Journal of Solar Energy Engineering 123 (4) (2001) 319–326.

[17] K. Selvam, S. Kanev, J. W. van Wingerden, T. van Engelen, M. Verhaegen, Feedback-feedforward individual pitch control for wind turbine load reduction, International Journal of Robust and Nonlinear Control 19 (1) (2008) 72–91.

[18] G. Bir, Multi-blade coordinate transformation and its applications to wind turbine analysis, in: AIAA Wind Energy Symposium, Reno, Nevada, 2008, pp. AIAA–2008–1300.

[19] J. Doyle, K. Glover, P. Khargonekar, B. Francis, State-space solutions to standard H_2 and H_∞ control problems, IEEE Transactions on Automatic Control 34 (8) (1989) 831–847.

[20] K. Zhou, J. C. Doyle, K. Glover, Robust and Optimal Control, 1st Edition, Prentice Hall, 1996.

[21] IEC 61400-1, Wind turbines-part 1: Design requirements, Tech. rep., International Electrotechnical Commission (8 2005).

[22] T. Burton, D. Sharpe, N. Jenkins, E. Bossanyi, Wind Energy Handbook, 1st Edition, John Wiley & Sons, 2001.

[23] B. Jonkman, TurbSim User's Guide, National Renewable Energy Laboratory, Golden, Colorado (2009).

[24] J. M. L. Buhl, MCrunch User's Guide, National Renewable Energy Laboratory, Golden, Colorado (2008).